Orbital-Free Density-Functional Theory Simulations of the Dynamic Structure Factor of Warm Dense Aluminum

T. G. White,[1,*] S. Richardson,[1,2] B. J. B. Crowley,[1,2] L. K. Pattison,[2] J. W. O. Harris,[2] and G. Gregori[1,†]

[1]*Department of Physics, University of Oxford, Parks Road, Oxford OX1 3PU, United Kingdom*

[2]*AWE, Aldermaston, Reading, Berkshire RG7 4PR, United Kingdom*

(Received 16 December 2012; published 24 October 2013)

Here, we report orbital-free density-functional theory (OF DFT) molecular dynamics simulations of the dynamic ion structure factor of warm solid density aluminum at $T = 0.5$ eV and $T = 5$ eV. We validate the OF DFT method in the warm dense matter regime through comparison of the static and thermodynamic properties with the more complete Kohn-Sham DFT. This extension of OF DFT to dynamic properties indicates that previously used models based on classical molecular dynamics may be inadequate to capture fully the low frequency dynamics of the response function.

DOI: 10.1103/PhysRevLett.111.175002 PACS numbers: 52.27.Gr, 52.40.Db, 52.65.Yy

The warm dense matter (WDM) regime defines a dense plasma state where strongly coupled classical ions coexist with partially or fully degenerate electrons [1]. The strong ion coupling and the quantum behavior of the electron fluid make simulation and modeling challenging, as traditional expansion techniques of classical plasma physics are no longer applicable and neither the kinetic nor the potential energy can be treated perturbatively. Such strongly interacting quantum many-body states of matter are found in the interiors of Jovian planets [2,3] and in the crusts of white dwarfs and neutron stars [4]. On Earth, they can be reproduced in the laboratory through the use of gas guns, pulsed power machines, diamond anvil cells, and through laser-plasma interactions [5,6], where they play an important role towards the success of inertial confinement fusion research [7].

A fundamental quantity, directly accessible to measurement, that describes the statistical and thermodynamic properties of the WDM state is the dynamic structure factor (DSF) [1]. For a system in thermodynamic equilibrium, the DSF gives its response to fluctuations of frequency ω and wave number $\mathbf{k}$, and is defined as

$$S(\mathbf{k}, \omega) = \frac{1}{2\pi N} \int e^{i\omega t} \langle \rho(\mathbf{k}, t) \rho(-\mathbf{k}, 0) \rangle dt, \qquad (1)$$

where N is the total number of particles, and $\langle \ldots \rangle$ refers to an ensemble average. Here, ρ is the Fourier transform of the real space time-dependent density distribution

$$\rho(\mathbf{k}, t) = \sum_{j=0}^{N} \exp[i\mathbf{k} \cdot \mathbf{r}_j(t)]. \qquad (2)$$

Since the x-ray scattering cross section is directly proportional to the DSF of the electrons [8,9], laboratory experiments can provide an important tool for the validation and verification of theoretical models of WDM [10,11].

Electrons in the plasma may occupy either free or bound states [12]; hence, the DSF contains features that are widely spread in frequency. On the high frequency side, it exhibits plasmon resonances which have been extensively discussed in the context of WDM and compared with x-ray scattering data from laser produced plasmas [8,13,14]. On the other hand, the ion-acoustic modes in the structure factor are separated by $2\hbar\omega_p \sim 10$–100 meV in most WDM states [11], where ω_p is the ion-plasma frequency. We refer to this low frequency part of the DSF as the ion-ion structure factor. The diagnosis of ion-acoustic dynamic modes in WDM has so far remained elusive due to the stringent requirements in photon number and bandwidth, which is considerably smaller than the bandwidth of any laser generated x-ray probe radiation. Accordingly, these modes cannot be resolved. In view of these limitations, most studies to date have concentrated on the evaluation of static (i.e., frequency integrated) structure factors with either semianalytical techniques or by solving the hypernetted chain equations [8,11,15–17]. Nevertheless, several questions on the intensity and spectral distribution of the ion-ion correlation function remain open [18]. These must be solved if accurate measurements of the equation of state are required. Also, since the ion-ion correlation function is related to the transport properties of the ions, knowledge of this term is essential for the understanding of the long-standing problem of energy equilibration in WDM [19–22].

Here, we present, for the first time, exact calculations of the ion-ion dynamic response that goes beyond approximate approaches used previously [1,23–25]. While a number of different theoretical approaches have been proposed to describe $S(k, \omega)$, where, in the case of an isotropic system, we can assume that the structure factors depend only on the absolute value $k \equiv |\mathbf{k}|$, none to date have used self-consistent quantum simulations.

Since an accurate calculation of the DSF requires ensemble averages over a large number of particles and long time scales, the full Kohn-Sham density-functional theory (KS DFT) still remains computationally prohibitive in

WDM regimes. The computational expense is due to the finite temperature treatment of electronic orbitals; these are filled according to the Fermi-Dirac distribution, which becomes smoother and broader as the temperature increases. Therefore, to capture the behavior of all thermally excited electrons requires a considerable number of partially filled states to be orthogonalized, a task that grows as the cube of the system size N. In order to take advantage of the largest possible number of particles in the simulation volume and maximize the computational speed, here we have instead adopted an orbital-free DFT (OF DFT) approach. In this technique, the electron energy functional is described entirely in terms of the electron density, without the need to solve for the wave functions.

The first step of our work consisted of comparing the static thermodynamic properties of the KS DFT and OF DFT results. All DFT simulations were performed using the ABINIT package [26–28]. We considered, as an example, a solid density aluminum plasma ($\rho = 2.7$ g cm^{-3}) with temperature $T = 0.5$ and $T = 5$ eV. The corresponding ion density is $n = 6.02 \times 10^{22}$ cm^{-3} with a Wigner-Seitz radius of $a = 2.99 a_B$ (a_B is the Bohr radius).

The KS DFT simulations were performed using the projector augmented wave framework [29]. To evolve the ion trajectories, we performed molecular dynamics simulations using a 108 ion cubic supercell in the isokinetic ensemble, with periodic boundary conditions applied. The kinetic energy was maintained constant through the use of a Gaussian thermostat. The cell was evolved to a simulation length up to 1 ps and in time steps of 2 fs. In each time step, the DFT equations for the electrons are solved in the Born-Oppenheimer approximation; ion positions are then updated classically according to the electrostatic forces computed from the known ion positions and the "frozen" electron charge density. The system is modeled in full thermodynamic equilibrium, with equal electron and ion temperatures. Brillouin zone sampling was performed at the mean value point [30]. Exchange and correlation (XC) were treated within the generalized gradient approximation of Perdew, Burke, and Ernzerhof [31]; electron interactions were described using a three valence electron projector augmented wave pseudopotential. The plane wave and augmentation cutoff energies were 952 and 2720 eV, respectively, ensuring convergence in the electronic density of states.

In OF DFT, the absence of electron wave functions requires that the kinetic energy must be a functional of electron density only. Our simulations were carried out using the Thomas-Fermi module of ABINIT with the XC terms treated within the local density approximation.

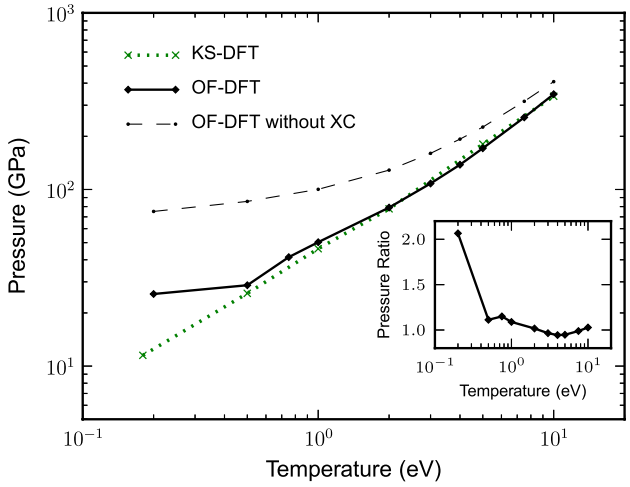

FIG. 1 (color online). Pressure of warm dense aluminum at solid density extracted from KS DFT (dotted line) and OF DFT (solid line). The two methods converge for $T \gtrsim 2$ eV. The convergence is highlighted by the inset, which shows the ratio between the OF DFT and KS DFT pressures. The dashed line represents OF DFT calculations performed without treating exchange and correlation, indicating the importance of these terms in this temperature regime.

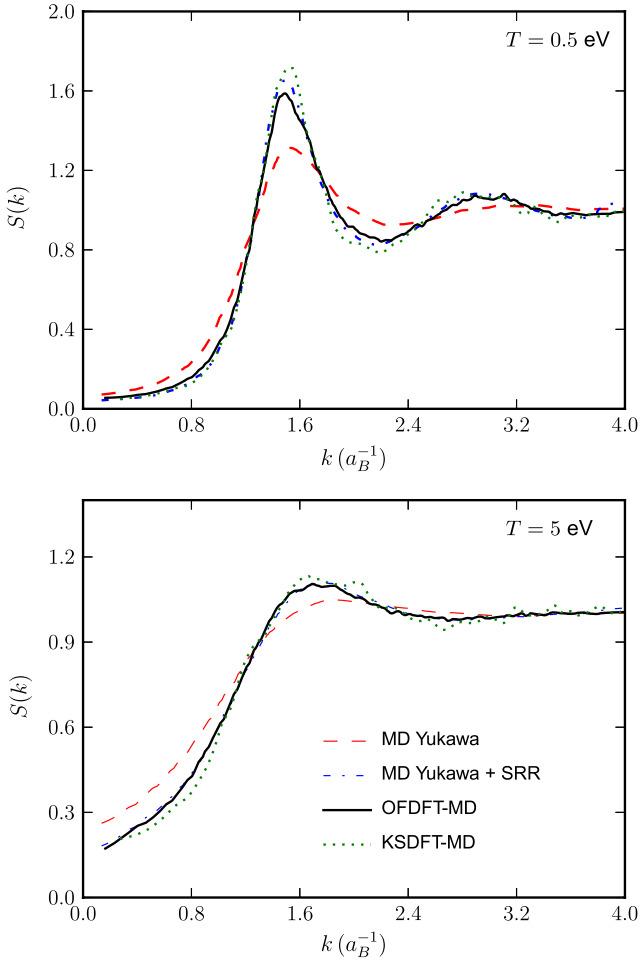

FIG. 2 (color online). The SSF for warm dense aluminum calculated from MD with the Yukawa potential (dashed line), Yukawa + SRR potential (dot-dashed line), OF DFT (solid line), and full KS DFT (dotted line). The results shown here are for $T = 0.5$ eV (top panel) and $T = 5$ eV (bottom panel).

The local density approximation and generalized gradient approximation have shown remarkable agreement in describing the properties of bulk aluminum [32] and are not expected to make significant differences to the dynamic or thermodynamic properties of the system. Replacing the kinetic energy functional introduces an error at lower temperatures where the system is dominated by bound electrons; we expect the error introduced to diminish with increasing temperature [33]. The OF DFT simulations contained 864 atoms and utilized a bulk-derived local pseudopotential. This pseudopotential was checked for accuracy by reproducing the electron density within a bulk material; details of this process and pseudopotential regularization can be found in Ref. [34]. Trajectories were evolved over a simulation length of 5 ps, using a time step of 0.25 fs. The time step was chosen to ensure energy conservation within the ion subsystem, while the simulation length was chosen to give high resolution DSF data. The DSF was then calculated using the final 1.5 ps of the simulation. Performing these calculations to the necessary accuracy requires considerable computational effort. Both the KS DFT and OF DFT simulations were performed using the massively parallel AWE supercomputer, Blackthorn.

Figure 1 compares the pressures calculated with both KS DFT and OF DFT over a range of temperatures and demonstrates that OF DFT reproduces well the KS DFT thermodynamic pressure above ≈ 2 eV. Also shown are OF DFT results that have not been corrected for XC. The relatively poor agreement of these data compared to the KS DFT calculations indicates the importance of including the XC term, as shown previously in Ref. [35]. Figure 2 also shows agreement between OF DFT and KS DFT in the static structure factor (SSF). Validation of the orbital-free approach through comparison with the static and thermodynamic properties has shown similar agreement in dense hydrogen plasmas [36] and liquid aluminum [37] but here is shown explicitly for the WDM region of phase space.

In addition to the DFT simulations, we have also considered a hybrid approach where the structure factor is extracted from a classical molecular dynamics (MD) simulation with an effective ion-ion potential given by [38]

$$V_{ii}^{\mathrm{eff}}(r) = \left[\frac{Z^2 e^2}{r} + \frac{(Z_c^2 - Z^2)e^2}{r} e^{-br}\right] e^{-\kappa r}, \qquad (3)$$

where $Z_c = 13$ is the atomic number for aluminum, $Z = 3$ is the charge state, and κ is the Thomas-Fermi screening length. The parameter b represents the effect of increased nuclear repulsion when there is interpenetration of the bound electron charge clouds around each nucleus. It determines the onset of the short-range repulsion (SRR). Setting $b \to \infty$ gives the usual Yukawa potential. The classical MD simulations were again run with 864 atoms in 0.2 fs time steps for a simulation time of 1.5 ps. We used the LAMPPS package [39] with a microcanonical ensemble and a velocity rescaling thermostat.

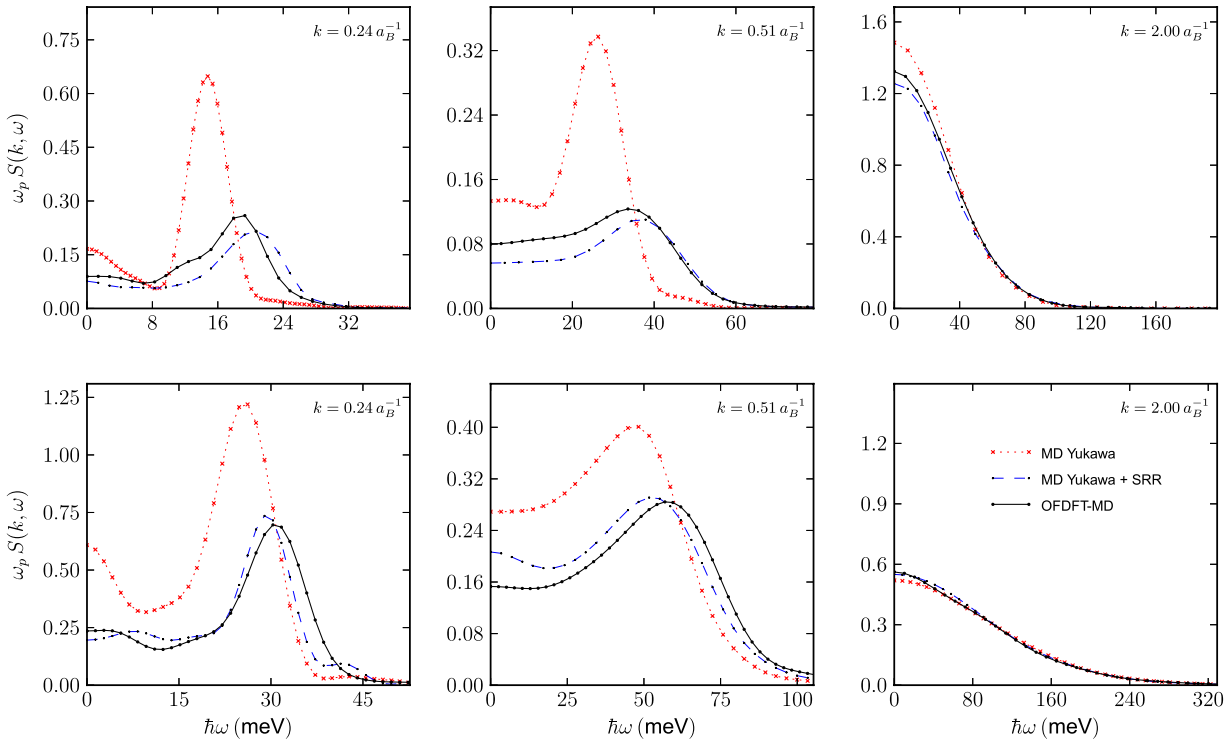

FIG. 3 (color online). The DSF for warm dense aluminum calculated from MD with the Yukawa potential (dotted line), Yukawa + SRR potential (dashed line), and OF DFT (solid line). The results shown here are for $T = 0.5$ eV (top panels) and $T = 5$ eV (bottom panels).

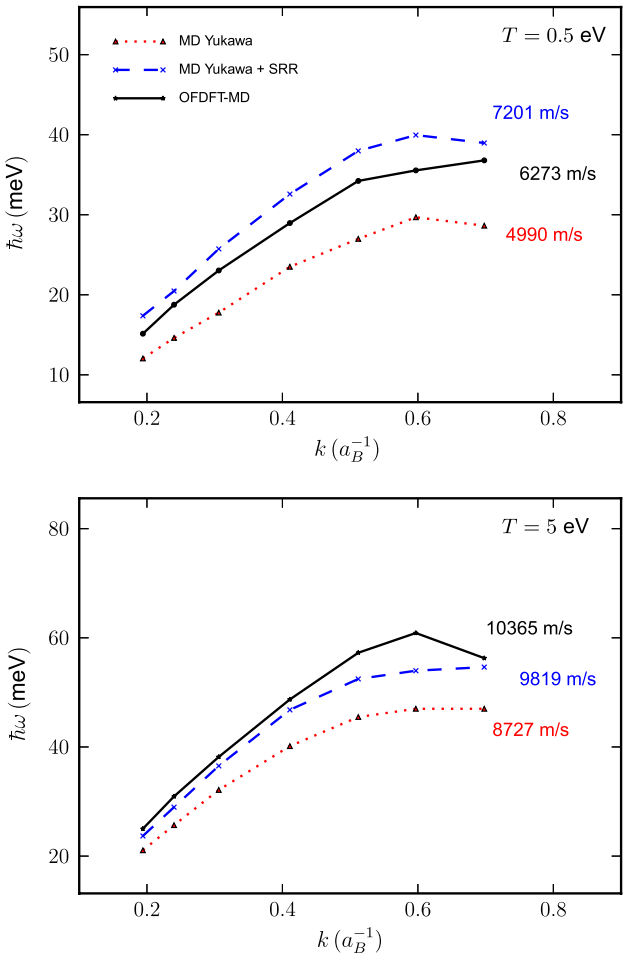

FIG. 4 (color online). The dispersion relation for warm dense aluminum calculated using OF DFT (solid line), MD with a Yukawa potential (dotted line), and MD with a Yukawa + SRR potential (dashed line). The results shown here are for $T = 0.5$ eV (top panel) and $T = 5$ eV (bottom panel). Also shown are the resulting sound speeds for each condition.

As discussed in Refs. [11,38], the parameter b can be determined by the requirement that the SSF obtained via classical MD simulations reproduce the KS DFT SSF. This is shown in Fig. 2. Classical MD simulations with the simpler Yukawa potential underestimate the correlation in the system when compared with the other methods. In Ref. [38], it was argued that it is indeed necessary to include the SRR term in the ion-ion potential in order for classical MD to match DFT simulations. In our situation, this is achieved by taking the parameter b to be $0.7a_B^{-1}$ and $1.12a_B^{-1}$ for $T = 0.5$ and $T = 5$ eV, respectively. On the other hand, OF DFT SSF compare very well with KS DFT results, without the need to introduce any adjustable parameters.

In Ref. [38], it was also suggested that the agreement between classical MD with a Yukawa + SRR potential and KS DFT in the SSF implies that MD simulations can then be used to calculate the DSF. However, while this approach does represent a significant step forward, compared to various semianalytical methods, it may not capture the response for the case of a time-dependent ion-ion interaction screened by a dynamical electron background. This is relevant to situations where the electron oscillations couple with ion-acoustic modes, as described through the plasmon-pole approximation [40,41]. Our OF DFT approach is instead able to include such effects in a consistent way, as the electron response is continuously updated in time throughout the simulation.

We have calculated the DSF $S(k, \omega)$ at three different values of k, to span the hydrodynamic ($k = 0.24a_B^{-1}$), generalized hydrodynamics ($k = 0.51a_B^{-1}$), and single-particle ($k = 2.0a_B^{-1}$) regimes [42]. The results of our calculations performed using OF DFT and classical MD simulations with both Yukawa and Yukawa + SRR potentials are presented in Fig. 3. In the large k regime, all models converge to the ideal gas result. However, at smaller values of k, the differences between the calculations are substantial. While classical MD simulations with a Yukawa + SRR potential agree better with OF DFT, there is still an important difference in the position of the ion-acoustic resonance. It is informative to plot the position of the peak of the resonance against the wave number, to yield the dispersion relation for these different models, as shown in Fig. 4. Differences in the dispersion relation result in different estimates to the sound speed, given by $d\omega/dk|_{k\to 0}$. The dispersion relation is assumed to be linear below $k = 0.2a_B^{-1}$. It is clear that for small k, the MD Yukawa + SRR potential matches well the OF DFT results. This regime corresponds to modes that have spatial correlations larger than the scale associated to SRR; here, we expect the fluctuation modes to be sensitive to the degree of SRR. However, as k increases and the correlation scale is reduced below that of the repulsion, the dispersion curves diverge, suggesting that the SRR correction is no longer adequate to describe the particle dynamics. At higher k still, the methods converge towards the single-particle regime, which is less sensitive to the specific form of the potential.

Although there is reasonable agreement between a classical MD simulation with a Yukawa + SRR potential and the OF DFT for warm dense aluminum, the applicability of the classical method is limited by the fact that the ion-ion potential must be known *a priori*. The proposed Yukawa form is not always reasonable, such as for metallized hydrogen [43] or molecular plasmas. Our OF DFT quantum simulations of the ion-ion structure factor provide a unique platform where dense plasma theory can be tested with high accuracy.

This work was partially supported by the EPSRC Grant No. EP/G007187/1 and by AWE PLC.

*thomas.white@physics.ox.ac.uk
†g.gregori1@physics.ox.ac.uk

[1] S. Ichimaru, Rev. Mod. Phys. **54**, 1017 (1982).
[2] T. Guillot, Science **286**, 72 (1999).

[3] G. I. Kerley, Phys. Earth Planet. Inter. **6**, 78 (1972).
[4] J. Daligault and S. Gupta, Astrophys. J. **703**, 994 (2009).
[5] M. D. Knudson, M. P. Desjarlais, and D. H. Dolan, Science **322**, 1822 (2008).
[6] W. J. Nellis, Rep. Prog. Phys. **69**, 1479 (2006).
[7] J. Lindl, Phys. Plasmas **2**, 3933 (1995).
[8] S. H. Glenzer and R. Redmer, Rev. Mod. Phys. **81**, 1625 (2009).
[9] B. J. B. Crowley and G. Gregori, New J. Phys. **15**, 015014 (2013).
[10] A. L. Kritcher *et al.*, Science **322**, 69 (2008).
[11] E. Garcia Saiz *et al.*, Nat. Phys. **4**, 940 (2008).
[12] J. Chihara, J. Phys. Condens. Matter **12**, 231 (2000).
[13] S. H. Glenzer, G. Gregori, R. W. Lee, F. J. Rogers, S. W. Pollaine, and O. L. Landen, Phys. Rev. Lett. **90**, 175002 (2003).
[14] S. H. Glenzer *et al.*, Phys. Rev. Lett. **98**, 065002 (2007).
[15] G. Gregori, S. H. Glenzer, W. Rozmus, R. W. Lee, and O. L. Landen, Phys. Rev. E **67**, 026412 (2003).
[16] M. W. C. Dharma-wardana and M. S. Murillo, Phys. Rev. E **77**, 026401 (2008).
[17] T. Ma *et al.*, Phys. Rev. Lett. **110**, 065001 (2013).
[18] K. Wünsch, J. Vorberger, and D. O. Gericke, Phys. Rev. E **79**, 010201(R) (2009).
[19] G. Gregori and D. O. Gericke, Europhys. Lett. **83**, 15 002 (2008).
[20] T. G. White *et al.*, Sci. Rep. **2**, 889 (2012).
[21] A. Ng, Int. J. Quantum Chem. **112**, 150 (2012).
[22] J. Daligault and G. Dimonte, Phys. Rev. E **79**, 056403 (2009).
[23] J.-P. Hansen and I. R. McDonald, *Theory of Simple Liquids* (Academic, London, 2000).
[24] A. A. Kugler, J. Stat. Phys. **12**, 35 (1975).
[25] G. Gregori and D. O. Gericke, Phys. Plasmas **16**, 056306 (2009).
[26] X. Gonze *et al.*, Comput. Phys. Commun. **180**, 2582 (2009).
[27] M. Torrent, F. Jollet, F. Bottin, G. Zérah, and X. Gonze, Comput. Mater. Sci. **42**, 337 (2008).
[28] F. Bottin, S. Leroux, A. Knyazev, and G. Zérah, Comput. Mater. Sci. **42**, 329 (2008).
[29] P. E. Blöchl, Phys. Rev. B **50**, 17 953 (1994).
[30] A. Baldereschi, Phys. Rev. B **7**, 5212 (1973).
[31] J. P. Perdew, K. Burke, and M. Ernzerhof, Phys. Rev. Lett. **77**, 3865 (1996).
[32] V. N. Staroverov, G. E. Scuseria, J. Tao, and J. P. Perdew, Phys. Rev. B **69**, 075102 (2004).
[33] F. R. Graziani *et al.*, High Energy Density Phys. **8**, 105 (2012).
[34] C. Huang and E. A. Carter, Phys. Chem. Chem. Phys. **10**, 7109 (2008).
[35] J. F. Danel, L. Kazandjian, and G. Zérah, Phys. Plasmas **19**, 122712 (2012).
[36] V. Recoules, F. Lambert, A. Decoster, B. Canaud, and J. Clérouin, Phys. Rev. Lett. **102**, 075002 (2009).
[37] J. A. Anta, B. J. Jesson, and P. A. Madden, Phys. Rev. B **58**, 6124 (1998).
[38] J. Vorberger, Z. Donko, I. M. Tkachenko, and D. O. Gericke, Phys. Rev. Lett. **109**, 225001 (2012).
[39] S. Plimpton, J. Comput. Phys. **117**, 1 (1995).
[40] J. Bardeen and D. Pines, Phys. Rev. **99**, 1140 (1955).
[41] N. W. Ashcroft and N. D. Mermin, *Solid State Physics* (Brooks-Cole, Belmont, MA, 1976).
[42] J. P. Mithen, J. Daligault, and G. Gregori, Phys. Rev. E **83**, 015401(R) (2011).
[43] S. T. Weir, A. C. Mitchell, and W. J. Nellis, Phys. Rev. Lett. **76**, 1860 (1996).